Journal of Cleaner Production 433 (2023) 139860

Contents lists available at ScienceDirect

Journal of Cleaner Production

journal homepage: www.elsevier.com/locate/jclepro

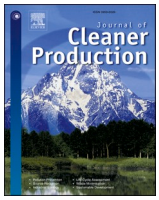

Downscaling CMIP6 climate projections to classify the future offshore wind energy resource in the Spanish territorial waters

B. Thomas [a,*], X. Costoya [a], M. deCastro [a], D. Insua-Costa [b,c], M. Senande-Rivera [c], M. Gómez-Gesteira [a]

[a] Centro de Investigación Mariña, Universidade de Vigo, Environmental Physics Laboratory (EPhysLab), Campus da Auga, 32004, Ourense, Spain
[b] Hydro-Climate Extremes Lab (H-CEL), Ghent University, Ghent, Belgium
[c] CRETUS Institute, Nonlinear Physics Group, Faculty of Physics, Universidade de Santiago de Compostela, Galicia, Spain

ARTICLE INFO

Handling Editor: Yuli Shan

Keywords:
Offshore wind energy
Climate change
CMIP6
Dynamical downscaling
WRF
Spanish maritime spatial planning

ABSTRACT

The Spanish government has established a Maritime Spatial Planning including areas for wind farms, with the aim of contributing up to 40% of European floating offshore wind power by 2030. Thus, it is crucial to assess the current and future offshore wind energy resource in these areas, and classify the near future resource by considering wind power density and other relevant factors like resource stability, environmental risks, and installation costs. To attain the necessary high spatial resolution, a dynamic downscaling of a multi-model ensemble from the 6th phase of the Coupled Model Intercomparison Project was conducted using the Weather Research and Forecasting model in Spanish territorial waters, including the Iberian Peninsula, Balearic Islands, and Canary Islands. Future projections were considered under the Shared Socioeconomic Pathways 2–4.5 and 5–8.5 scenarios. According to the results, Spain's offshore wind energy potential is projected to grow in the upcoming years, particularly in the Atlantic Ocean and surrounding the Canary Islands. Wind resource classification in the potential offshore wind farm areas reveals noteworthy diversity, with ratings ranging from "fair" (3/7) to "outstanding" (6/7). The most promising areas for offshore wind farm development in the near future are located in the northwest of the Iberian Peninsula and the Canary Islands.

1. Introduction

The use of fossil fuels as a primary source of energy has an undeniable and significant impact on the Earth's climate change, through the emission of greenhouse gases (GHGs) (IPCC, 2021). In 2021, during the COP26 conference in Glasgow, the United Nations emphasized the urgent need to reduce the net CO_2 emissions to zero by 2050 to prevent the average temperature of the planet from rising beyond +2 °C (United Nations, 2021). Therefore, it has become essential to generate "clean energy" that does not emit GHGs in order to mitigate the adverse effects of human activities on the climate. Renewable energy sources offer a potent solution to accomplish this goal and are currently undergoing a remarkable expansion. Globally, their cumulative capacity surged from 175 GW in 2017 to 335 GW in 2022, thus representing a 90% increase in a few years (IEA, 2023).

Among renewable energy sources, wind energy has already established itself as a leading contender in Europe, owing to the deployment of wind turbines on the mainland, a technology that has been proven to be efficient and mature (WindEurope, 2023a). However, offshore wind energy, which involves installing wind turbines in the sea, is expected to play a crucial role in the coming years and decades (GWEC, 2023; WindEurope, 2023b). This is because the oceans constitute 70% of the Earth's surface and offer higher and more consistent wind speeds than those on the mainland (BOEM, n.d.). Additionally, modern offshore wind turbines can float by being installed on anchored buoys rather than being built directly on the ocean floor. Therefore, they can be installed at greater water depths, making it possible for offshore wind farms to be more uniformly distributed across Europe in the future. Presently, the North Sea boasts the highest density of offshore wind farms globally (GWEC, 2020), while other regions like the Iberian Peninsula have not yet harnessed this renewable energy due to their narrow continental shelf.

It's worth noting that while offshore wind energy can help reduce the impact of climate change, it can also be affected by it. Indeed, wind power is dependent on the cubed wind speed (Costoya et al., 2020a; Santos et al., 2018). Thus, even slight variations in wind speed, caused by climate change, can have a significant impact on wind power. For

* Corresponding author.
E-mail address: brieuc.thomas@uvigo.es (B. Thomas).

https://doi.org/10.1016/j.jclepro.2023.139860
Received 7 July 2023; Received in revised form 15 November 2023; Accepted 19 November 2023
Available online 23 November 2023

Nomenclature

CMIP6	6th phase of the Coupled Model Intercomparison Project
CORDEX	Coordinated Regional Climate Downscaling Experiment
C_v	Temporal Stability
DC	Distance to Coast
EWS	Extreme Wind Speed
EWSO	Effective Wind Speed Occurrence
GCM	General Circulation Model
GHGs	Greenhouse Gases
MSP	Maritime Spatial Planning
M_v	Monthly Stability
OP	Overlapping Percentage
RCM	Regional Climate Model
RLO	Rich Level Occurrence
SSP	Shared Socioeconomic Pathway
W10 and W100	Wind Speed at 10 and 100 m above sea level
W_{ann}	Average Annual Wind Speed
WD	Water Depth
WPD	Wind Power Density
WRF	Weather Research and Forecasting

example, a decrease of the wind speed from 10 m s^{-1} to 9 m s^{-1} (-10%) would result in a 27% decrease in wind power. As the installation of offshore wind farms is expected to increase rapidly in the coming years, it's crucial to understand how climate change could alter wind speed patterns. Climate models have proved to be the most suitable and robust tool to achieve this (Fernández-Alvarez et al., 2023; González et al., 2017; Zhang and Li, 2021). The 6th phase of the Coupled Model Intercomparison Project (CMIP6) (Eyring et al., 2016) provides the most recent and extensive collection of General Circulation Models (GCMs), which offer climate projections of the atmosphere based on different scenarios of future GHG emissions, referred to as Shared Socioeconomic Pathways (SSPs) (Riahi et al., 2017). These scenarios consider various policies that take into account different hypotheses about the evolution of population, education, urbanization, and Gross Domestic Product (GDP) to assess future GHG emissions. However, these GCMs offer a relatively coarse resolution since they model the entire atmosphere of the Earth, making it difficult to study the impact of climate change in specific regions. Therefore, it's necessary to increase the spatial resolution of these models to carry out more detailed analyses at the regional scale. This can be accomplished through dynamical downscaling using Regional Climate Models (RCMs), which are forced with GCMs data and enable the modeling of the atmosphere with a much better resolution, taking into account the specific characteristics of the area under study. Nevertheless, analyzing the reliability of climate models in accurately replicating wind patterns within a particular region is of paramount importance. This entails a comparison between historical model simulations and observational data specific to the area. Models that demonstrate a statistically significant alignment with observed data are regarded as robust in replicating the region's reality, thus rendering their future simulations suitable for assessing forthcoming wind patterns.

The investigation into the impact of climate change on offshore wind energy is particularly relevant in Spanish territorial waters, which includes the Iberian Peninsula, Balearic Islands, and Canary Islands, due to the expected rapid growth of offshore wind energy production in the country. The Spanish government has set a target of achieving an installed offshore wind capacity between 1 and 3 GW by 2030, which could contribute up to 40% of the European targets for floating offshore wind (Spanish Ministry for Ecological Transition and the Demographical Challenge, 2022). To achieve this goal, the Spanish government has recently published a Maritime Spatial Planning (MSP) including 19 areas where offshore wind farms could be installed (blue polygons in Fig. 1), divided into four zones (NOR, LEBA, ESAL, and CAN) (Spanish Ministry for Ecological Transition and the Demographical Challenge, 2023). This indicates that the legal framework for offshore wind energy in Spain is now well-defined. It should be noted that the definition of a MSP is a key tool in order to permit the development of offshore wind energy harnessing, thus all of the coastal European countries defined one of their own (WindEurope, 2022). In addition, the high offshore wind energy resource potential in the Spanish territorial waters, particularly on the Atlantic coast (Costoya et al., 2020a, 2022; Salvação and Guedes Soares, 2018), and technical advances in floating wind turbines, which have allowed for the installation of the first offshore floating wind farm in Portugal (https://www.edp.com/en/innovation/windfloat), are other positive factors. It is worth emphasizing that designing a Maritime Spatial Planning (MSP) for floating offshore wind facilities involves the consideration of numerous factors. These include the assessment of wind resources, wave conditions, proximity to the shoreline, and the need to avoid navigational routes and protected areas (Díaz et al., 2019).

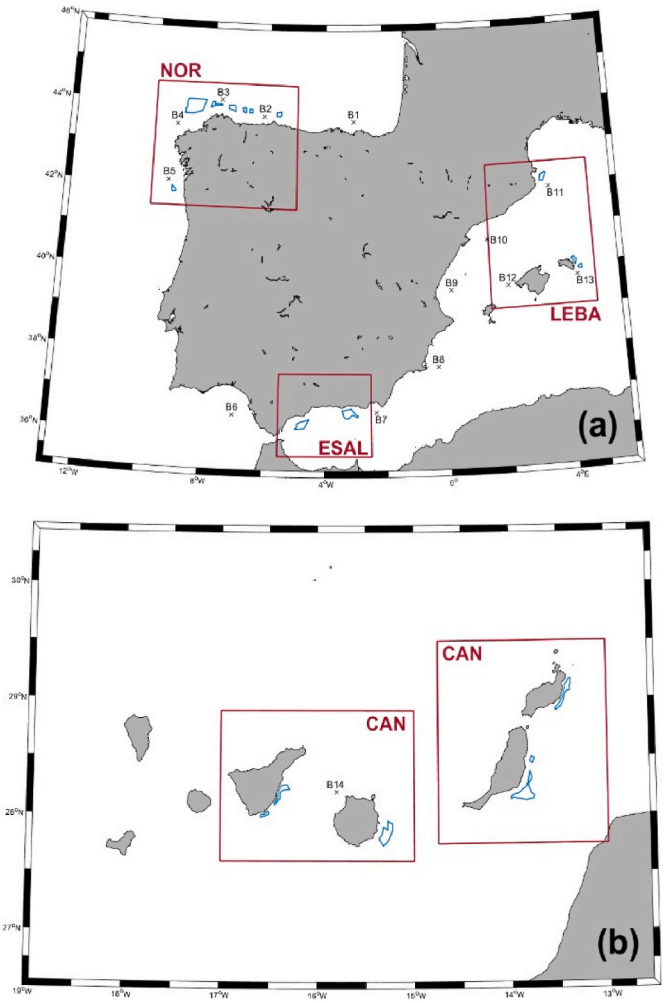

Fig. 1. Area under scope of this study: **(a)** Continental Spain and Balearic Islands, **(b)** Canary Islands. Red shapes mark the zones containing polygons (painted in blue color) where it is possible to install offshore wind farms. Numbered crosses indicate the location of buoys from Puertos del Estado.

Previous studies have assessed the impact of climate change on wind speed patterns within the Spanish territorial waters. Fernández-Alvarez et al. (2023) studied offshore wind climate projections in the western

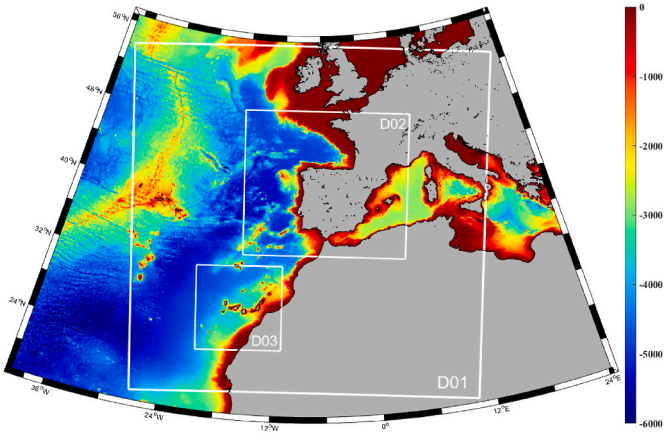

Fig. 2. Bathymetry (m) of the region of study and simulation domains (white lines) used in WRF.

Iberian Peninsula using the WRF (Weather Research and Forecasting) model to downscale CESM2 GCM data from CMIP6. They found that Wind Power Density (WPD) is predicted to increase during the 21st century, particularly during summer. Conversely, Costoya et al. (2020a) observed a decrease in WPD on the Atlantic coast of the Iberian Peninsula, except for the North West corner, with an increase projected during summer in the 21st century. They bias-corrected the downscaled Coordinated Regional Climate Downscaling Experiment (CORDEX) data obtained with CMIP5 coarse data. Soares et al. (2017) detected a general reduction in wind resources within the western Iberian Peninsula, except for summer, using both CORDEX data and a WRF dynamical downscaling of EC-EARTH GCM from CMIP5. Lastly, using CORDEX data, Santos et al. (2018) identified that, except for Galicia, the Strait of Gibraltar, and Cape Gata, where offshore resources are predicted to increase, a general decrease in wind resources is anticipated throughout the Iberian Peninsula. In the Canary Islands, González et al. (2017) conducted a study to analyze the development of wind speed patterns using a WRF dynamical downscaling of CMIP5 data. They found that the WPD is expected to increase in some areas and decrease in others due to the significant influence of the islands' topographies. In addition, previous studies have examined other aspects related to offshore wind energy. For instance, economic feasibility (Castro-Santos and Diaz-Casas, 2015; Castro-Santos et al., 2016) of installing offshore wind farms, particularly in the northwest of the Iberian Peninsula, has been explored. Additionally, legislation surrounding these installations has also been analyzed for this area (Rodríguez-Rodríguez et al., 2016; Salvador et al., 2018).

Climate change's impact on offshore wind energy resources has been studied in other regions using CMIP6 data. Martinez et al. (2023) investigated the future WPD projections in Northern Europe by using raw data from multiple CMIP6 GCMs with coarse resolution and predicted a general decrease in WPD. Zhang and Li (2021) conducted a study on future offshore wind projections in China using a deep learning downscaling of CMIP6 data. They discovered that an increase in WPD is expected over the South China Sea and a decrease over the East China Sea. Lastly, Carvalho et al. (2021) outlined several differences in wind energy resource between CMIP5 and CMIP6 future climate projections in Europe. As an example, CMIP6 projects a decline for almost all Europe by the end of the century, especially under SSP5-8.5, whereas CMIP5 predicted an increase in Northern Europe.

This study aims to achieve two main objectives. First, to evaluate the impact of climate change on the future wind energy resource in areas designated by the Spanish Government's MSP to host wind turbine farms. Secondly, to classify the offshore wind energy resource in these zones, considering various crucial factors for installing offshore wind turbines. This approach will identify areas with the most favorable conditions for installing offshore wind farms within the current legal framework. The study will employ data from a dynamical downscaling of a CMIP6 multimodel under two future scenarios, SSP2-4.5 (intermediate GHGs emissions) and SSP5-8.5 (high GHGs emissions), representing the latest future projections. The dynamical downscaling will be carried out using the WRF-ARW v4.3.3 model (referred as WRF). To the best of our knowledge, this study is the first to analyze and classify future offshore wind energy in the areas of the Spanish territorial waters designated for offshore wind farms under the current legal framework.

2. Data and Methods

This section details the procedures employed to acquire the wind data necessary for this analysis, along with the methodologies used to validate the results and classify offshore wind energy. Initially, it describes the parametrization used in the WRF model to dynamically downscale the CMIP6 data. Subsequently, it explains the process of comparing results with reanalysis and observational data for validation purposes. Finally, it elucidates the methodology used to classify the offshore wind data, facilitating the identification of optimal locations for harnessing wind energy.

2.1. WRF model setup

The wind speed, a crucial variable for wind energy calculations, was obtained by means of a dynamical downscaling approach using the WRF-ARW v4.3.3 meteorological model (Skamarock et al., 2021). The initial and boundary conditions were provided by Xu et al. (2021) with a spatial resolution of 1.25° and a temporal resolution of 6 h. This data set covers a historical period from 1985 to 2014 and a future period from 2015 to 2100 under SSP2-4.5 and SSP5-8.5 scenarios. The database considers a multi-model ensemble of 18 GCMs from CMIP6 project for long-term trend, and the internal climate variability of a single CMIP6 model (MPI-ESM1-HR). In addition, the dataset was biased corrected using data from the ERA5 reanalysis (Hersbach et al., 2020) for the period 1979–2014. To summarize the process for obtaining these data, Xu et al. (2021) used data from one of the CMIP6 GCMs (MPI-ESM1-HR) and decomposed it into a non-linear long-term and an inter-annual perturbation term. Then, they corrected the MPI-ESM1-HR variance bias by correcting the inter-annual perturbation term using the variance of the ERA5 data over the historical period (1979–2014). Next, they corrected the non-linear long-term by using the non-linear long-term of the multi-model ensemble instead of the one of a single GCM. Lastly, they bias-corrected the GCM by removing to the data the subtraction between the mean bias of the long-term trend of the GCM data and the one of the ERA5 reanalysis dataset, over the historical period.

WRF was configured with three different simulation domains. The parent domain, referred to as D01 in Fig. 2, had a spatial resolution of 30 km, while for the two nested domains, D02 and D03, a spatial resolution of 10 km was used. D02 covered continental Spain and the Balearic Islands, while D03 covered the Canary Islands. The use of this configuration allowed the generation of future wind speed data with the necessary spatial resolution to conduct a detailed analysis of the areas designated for offshore wind farm installation in the whole Spanish coast.

Three 30-year climate periods were simulated: historical (1985–2014), near future (2030–2059) and far future (2070–2099), under two scenarios: SSP2-4.5 and SSP5-8.5. To prevent errors from accumulating in the WRF model, the simulations were run on a daily basis with a spin-up period of 12 h. This means that each simulation lasted 36 h, starting at 12:00 UTC on the previous day of interest. This method, which has been used in previous studies using the WRF model for downscaling (Horvath et al., 2012; Jerez et al., 2020; Lo et al., 2008; Pan et al., 1999; Qian et al., 2003), ensures greater accuracy at the cost of higher computational resources compared to continuous simulations of the entire period. In addition, the following parameterizations were

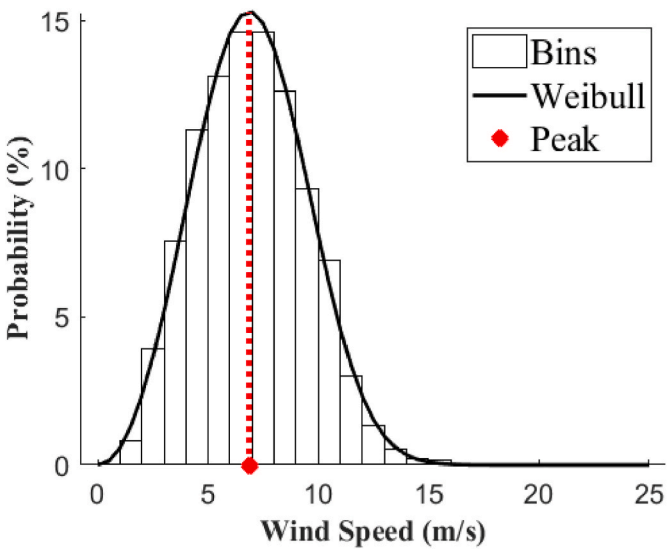

Fig. 3. Tools used during the validation process for each wind speed series. White bars represent the frequency of occurrence of wind speed for each bin used to calculate the OP, black line is the closest Weibull distribution, and red mark is the location of its maximum on the X axis. Data from the WRF historical simulation in D02, at location [7.6936°W; 44.1008°N].

used: Thompson microphysics scheme (Thompson et al., 2008), Yonsei University planetary boundary layer scheme (Hong et al., 2006), United Noah land surface model (Tewari et al., 2004), Revised MM5 surface layer scheme (Jiménez et al., 2012), RRTMG shortwave and longwave radiations scheme (Iacono et al., 2008) and New Tiedtke cumulus parametrization (Zhang and Wang, 2017).

The simulation output provided wind speed data at two different heights above sea level, namely, 10 m and 100 m (denoted as W10 and W100, respectively) with a temporal resolution of 6 h and a spatial resolution of 10 km (within the areas of interest, as shown in Fig. 1). While W100 was the primary variable of interest due to its relevance for wind turbines' hub height, W10 was also considered for validation with observed data.

2.2. Validation of WRF outputs

To evaluate the accuracy of simulated wind speed, two separate validations were conducted using different datasets. Firstly, the W100 outputs from WRF simulations were compared with ERA5 wind speed values (Hersbach et al., 2020) at 100 m, encompassing the entire region of continental Spain, Balearic Islands, and Canary Islands. The ERA5 data between 1985 and 2014, with a spatial resolution of 0.25° and 1-h temporal resolution, was used for this purpose, which was obtained from: https://cds.climate.copernicus.eu/cdsapp#!/dataset/reanalysis-era5-single-levels?tab=form. To compare the W100 data from WRF and ERA5 for the historical period, the overlapping percentage (OP, Perkins et al., 2007) between all grid points from both datasets was calculated in the areas under scope, as shown in Fig. 1. Since the WRF and ERA5 datasets have different spatial resolutions, a linear interpolation of the WRF grid (higher resolution, 10 km) on the ERA5 grid (lower resolution, 0.25°) was performed, solely for this validation process. Additionally, the two datasets do not have the same temporal resolution, and hence daily mean values were calculated for both datasets. Then, the probability density function of each series of W100 was computed for each grid point, using 25 bins (from 0 to 25 m s^{-1} with a 1 m s^{-1} increment) for both datasets. Fig. 3 illustrates an example of this process visually.

Finally, the OP of each grid point is calculated with the following formula:

$$OP(\%) = 100 * \sum_{i=1}^{n} minimum\left(Z_i^{WRF}, Z_i^{Valid}\right) \quad (1)$$

Here, n represents the number of bins (25) and Z_i is the frequency of occurrence of the wind speed range between (i-1) and (i) m.s^{-1}, of WRF or "Valid" (here ERA5) dataset.

The second validation involved using observed data from 14 buoys located in the same area under scope. These buoys measured wind speed at 3 m above sea level with an hourly temporal resolution (except for buoys B1 and B13, which have a 3-h temporal resolution until 2002 and 2004, respectively) and were selected from Puertos del Estado (https://www.puertos.es/es-es) as shown in Table 1. The period that was processed for comparison with WRF simulated data ranged from the starting year of recording of each buoy (see Table 1) to 2014. For each buoy, the number of available measurements within this period is also shown in Table 1. The locations of these buoys were represented by numbered crosses in Fig. 1.

Formula 2 had to be applied to extrapolate the wind speed from the buoys, which was measured at a height of 3 m above sea level, to a height of 10 m above sea level for the validation process (Santos et al., 2018).

$$W_{H_2} = W_{H_1} * \frac{\ln\left(\frac{H_2}{z_0}\right)}{\ln\left(\frac{H_1}{z_0}\right)} \quad (2)$$

Where, H_1 is the height at which data is available, H_2 is the height at which data is extrapolated, W_{Hi} is the wind speed at the height H_i, and z_0 is the roughness length of the terrain. In this case, $H_1 = 3$ m and $H_2 = 10$ m, therefore W_{H1} is the raw data obtained from buoys, while W_{H2} is the extrapolated wind speed at 10 m above sea level that will be used for the comparison with WRF data. The roughness length of the ocean's surface

Table 1
Buoys from Puertos del Estado (https://www.puertos.es/es-es) used in this study, spanning from the starting year to 2014.

Number	Name	Longitude (°)	Latitude (°)	Starting year	N° Measurements
B1	Bilbao-Vizcaya	−3.04	43.64	1990	120,185
B2	Cabo de Peñas	−6.18	43.75	1998	126,849
B3	Estaca de Bares	−7.68	44.12	1996	121,314
B4	Villano-Sisargas	−9.21	43.5	1998	121,013
B5	Cabo Silleiro	−9.43	42.12	1998	128,518
B6	Golfo de Cadiz	−6.96	36.49	1996	149,972
B7	Cabo de Gata	−2.34	36.57	1998	120,094
B8	Cabo de Palos	−0.31	37.65	2006	71,534
B9	Valencia	0.20	39.51	2005	74,366
B10	Tarragona	1.47	40.69	2004	86,484
B11	Cabo de Begur	3.65	41.9	2001	94,060
B12	Dragoneras	2.10	39.56	2006	67,364
B13	Mahón	4.42	39.71	1993	100,021
B14	Gran Canaria	−15.8	28.2	1997	135,091

Table 2
Weight given to each one of the eight normalized indices.

	W_{ann}	EWSO	RLO	C_v	M_v	EWS	DC	WD
Weight	0.22	0.22	0.10	0.10	0.05	0.14	0.07	0.10

Table 3
Classification given to the resource according to the final index.

Class	Index value	Resource potential
1	⩽ 0.4	Poor
2	(0.4, 0.5]	Marginal
3	(0.5, 0.6]	Fair
4	(0.6, 0.7]	Good
5	(0.7, 0.8]	Excellent
6	(0.8, 0.9]	Outstanding
7	>0.9	Superb

was set at $z_0 = 1.52\ 10^{-4}$ m as in previous studies (Peixoto and Oort, 1992). Since the temporal resolutions of the WRF and buoy data are different, daily averaged values of wind speed are calculated for both data sets. The closest point of the WRF grid to each buoy is then determined and used to compare the two series of W10. To validate the results, three different metrics were used. The first metric was the OP, which was calculated using the methodology described previously (Formula 1, with "Valid" = "Buoy"). The second metric involved calculating the percentage of difference between the medians of the two series using the following formula (Costoya et al., 2020a):

$$\Delta Med\ (\%) = 100 * \frac{Med_{WRF} - Med_{Buoy}}{Med_{Buoy}} \tag{3}$$

Finally, the percentage of difference in the peak location of the Weibull distribution between the two series was considered (Formula 4, Costoya et al., 2020a). This involved computing the closest Weibull distribution for both series and comparing the locations of the peaks on the X-axis (as shown in Fig. 3).

$$\Delta Peak\ (\%) = 100 * \frac{Peak_{WRF} - Peak_{Buoy}}{Peak_{Buoy}} \tag{4}$$

Consequently, two types of validation were conducted. The first type involved considering the entire scope of the area under examination using ERA5 data. The second type involved the use of observational data to validate WRF simulations for specific locations. Both validation approaches were used complementarily.

2.3. Wind power density calculation

The output data from WRF model is wind speed, but wind energy values are needed in order to evaluate the potential for harnessing this resource. To this end, Formula 5 (Santos et al., 2018) is used to calculate wind power density:

$$WPD = \frac{1}{2}\rho_a W^3 \tag{5}$$

Where ρ_a is the air density (1.225 kg m^{-3} at 288.15 K and 1000 hPa), W ($m.s^{-1}$) is the wind speed and WPD ($W.m^{-2}$) is the wind power density.

To depict the changes in wind power density (ΔWPD) between historical and future periods, the percentage difference between the average values of the two periods is computed using the following formula:

$$\Delta WPD(\%) = 100 * \frac{WPD_{fut} - WPD_{hist}}{WPD_{hist}} \tag{6}$$

2.4. Wind resource classification

When analyzing the suitability of coastal locations for installing offshore wind farms, wind power density (WPD) is not the only parameter to be taken into consideration. Other parameters related to the resource's richness, stability, risk to oceanic structures, and economic costs should also be included. As a result, the offshore wind energy resource in all polygons within the Spanish MSP was classified, providing a more comprehensive understanding of the suitability of areas for offshore wind farm installation. The classification process considered eight different indices, accounting for the richness and stability of the resource, risk to oceanic structures, and economic costs. A similar methodology has previously been applied in other areas for both offshore wind energy resource (Costoya et al., 2019, 2020b, 2021, 2022; Zheng and Pan, 2014; Zheng et al., 2018) and wave energy (Ribeiro et al., 2021). In this study, the methodology proposed by Costoya et al. (2022) will be followed.

To assess the richness of the resource, three different indices were established. The first index is the W_{ann} ($m.s^{-1}$), which considers the average annual wind speed value. The second index, Effective Wind Speed Occurrence (EWSO, %), represents the percentage of time during which wind speeds are between 4 m s^{-1} and 25 m s^{-1}, the cut-in and cut-out wind speeds, respectively, at which a wind turbine can generate energy. The final index is the Rich Level Occurrence (RLO, %), which indicates the percentage of time during which the WPD is higher than 200 W m^{-2}. To evaluate the stability of the resource, two other indices were utilized. The first is C_v, which is a measure of temporal stability that is defined using the standard deviation (σ) and the mean value ($\overline{W}$) of the wind speed data over all the considered period of simulation, as shown in Formula 7. The second index is M_v, which is an index of monthly stability that is defined using the mean WPD of the least and most energetic months in the climatic year (WPD_{M12} and WPD_{M1}, respectively), as well as the mean annual WPD ($\overline{WPD}$), as demonstrated in Formula 8.

$$C_v = \frac{\sigma}{\overline{W}} \tag{7}$$

$$M_v = \frac{WPD_{M1} - WPD_{M12}}{\overline{WPD}} \tag{8}$$

To assess the risk to oceanic structures, the Extreme Wind Speed (EWS in $m.s^{-1}$) index is also utilized, which is associated with the highest wind speed value that can be found over all the considered period of simulation. Indeed, extreme winds might harm wind turbine structures. This index is calculated using a Gumbel curve method with a 50-year return period (Zheng et al., 2018).

Finally, the economic cost is evaluated using two indices: the distance to the coast (DC in degrees) and the water depth (WD in meters). Building an offshore wind turbine closer to the coast and in shallower waters is less expensive.

This entire methodology used a Delphi approach. Thus, several experts, scientists and engineers working in this field have been asked what aspects would most affect the use of offshore wind energy, and then they have given a weight to each of these indices. Detailed information of this part of the methodology can be seen in Zheng et al. (2018). Nevertheless, these eight indices used in the analysis have different units and magnitudes, and therefore must be normalized to allow for comparison between them. To achieve this, several normalization methods were applied, following the values of Tables A1 to A3 (Appendix section). These normalization methods produced normalized indices with values between 0 (worst) and 1 (best), and without units.

To obtain a single index for each location, the normalized indices were combined with different weights provided by the experts consulted before, as described in Table 2. The resulting final index represents the sum of each normalized index multiplied by its respective weight. The values of the final index were then used to classify the areas based on

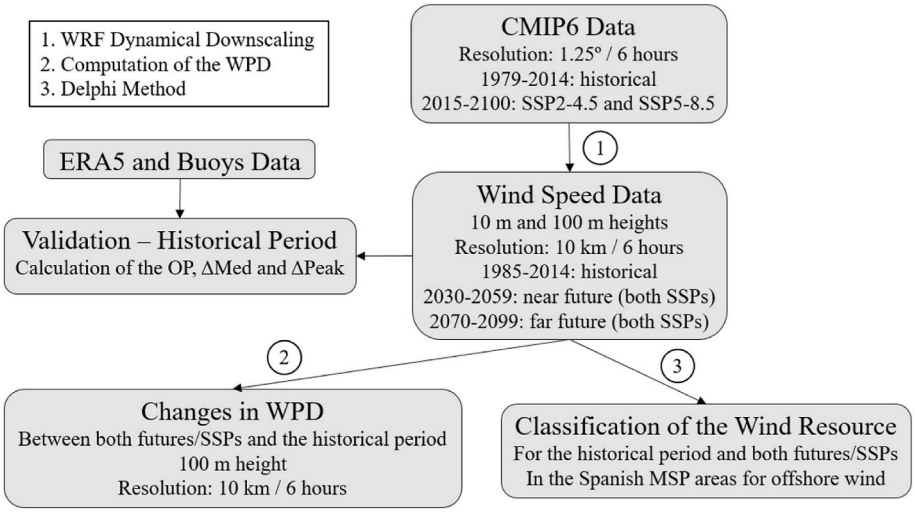

Fig. 4. Flowchart of the processes described in Data and Methods section.

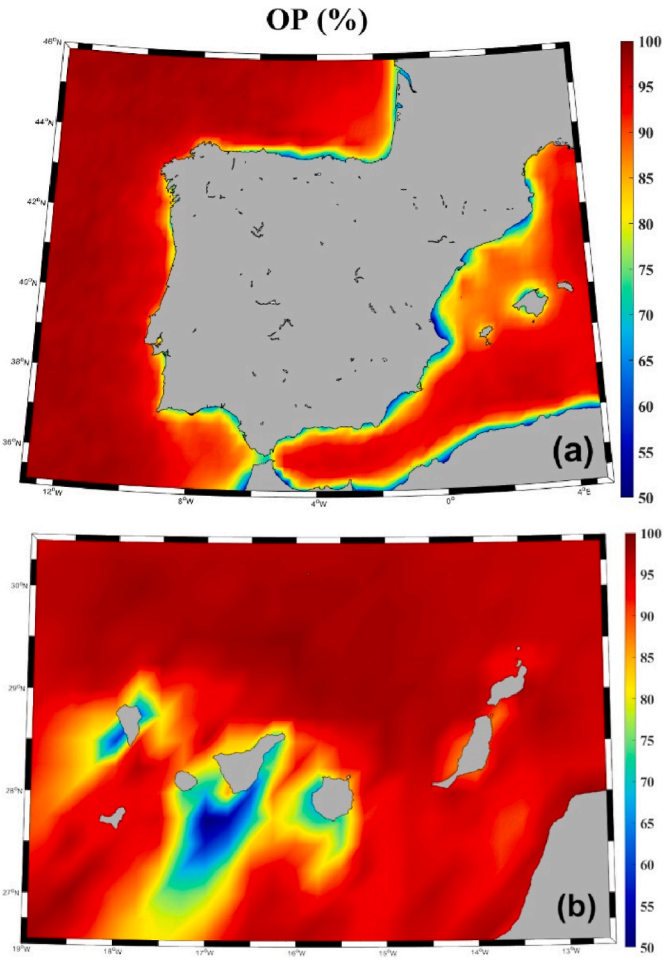

Fig. 5. OP (%) between W100 from WRF simulation and ERA5 dataset, for the 1985–2014 period in the: **(a)** Continental Spain and Balearic Islands, **(b)** Canary Islands.

their suitability for offshore wind farms, as presented in Table 3. The values for Tables 2 and 3 correspond to the ones found in various studies (Costoya et al., 2019, 2020b, 2021, 2022; Zheng and Pan, 2014; Zheng et al., 2018).

Fig. 4 summarizes all the data and Method section of this analysis.

Table 4
Metrics of comparison between W10 from WRF simulation and Puertos de Estado's buoys.

Buoy n°	OP (%)	**ΔMed** (%)	**ΔPeak** (%)
B1	93.6	3.1	6.6
B2	94.4	0.3	1.8
B3	94.7	0.4	2.9
B4	93.3	9.2	12.0
B5	90.3	9.3	16.4
B6	89.6	12.0	15.2
B7	88.2	18.9	23.4
B8	83.9	21.5	30.5
B9	86.2	11.7	21. 0
B10	87.4	18.2	29.4
B11	85.3	13.2	29.8
B12	86.2	16.3	24.0
B13	94.1	5.6	11.4
B14	91.8	−5.8	−6.8
Mean ± STD	**89.9 ± 3.7**	**9.6 ± 8.0**	**15.5 ± 11.6**

3. Results and discussion

In this section, the study presents various results obtained. Initially, it relates the validation of dynamically downscaled data, comparing it to reanalysis (ERA5) and observational (buoys) data. Subsequently, it provides a detailed account of the distribution of WPD in Spanish territorial waters in the historical period, along with its evolution in the near future. Finally, it frames the classification of the offshore wind resource within the 19 polygons defined by the Spanish MSP, for both the historical and near future periods.

3.1. Validation of the WRF simulations

To verify the accuracy of the data used in this research, two comparisons were conducted between the WRF model output and observational data for the historical period (1985–2014). Initially, the W100 output from WRF was compared with the W100 data from the ERA5 reanalysis dataset by computing the Overlapping Percentage (OP, Formula 1) between the two variables. The findings are presented in Fig. 5. In general, values of OP are greater than 90% in open sea and slightly lower closer to the coast. However, at the south of Tenerife Island in the Canary Islands domain (Fig. 5b), the OP values are lower than 60%, possibly due to the interactions between northeast trade winds and the Teide mountain at the center of the island. Indeed, the lower resolution of the ERA5 data set (in comparison with the WRF simulations carried

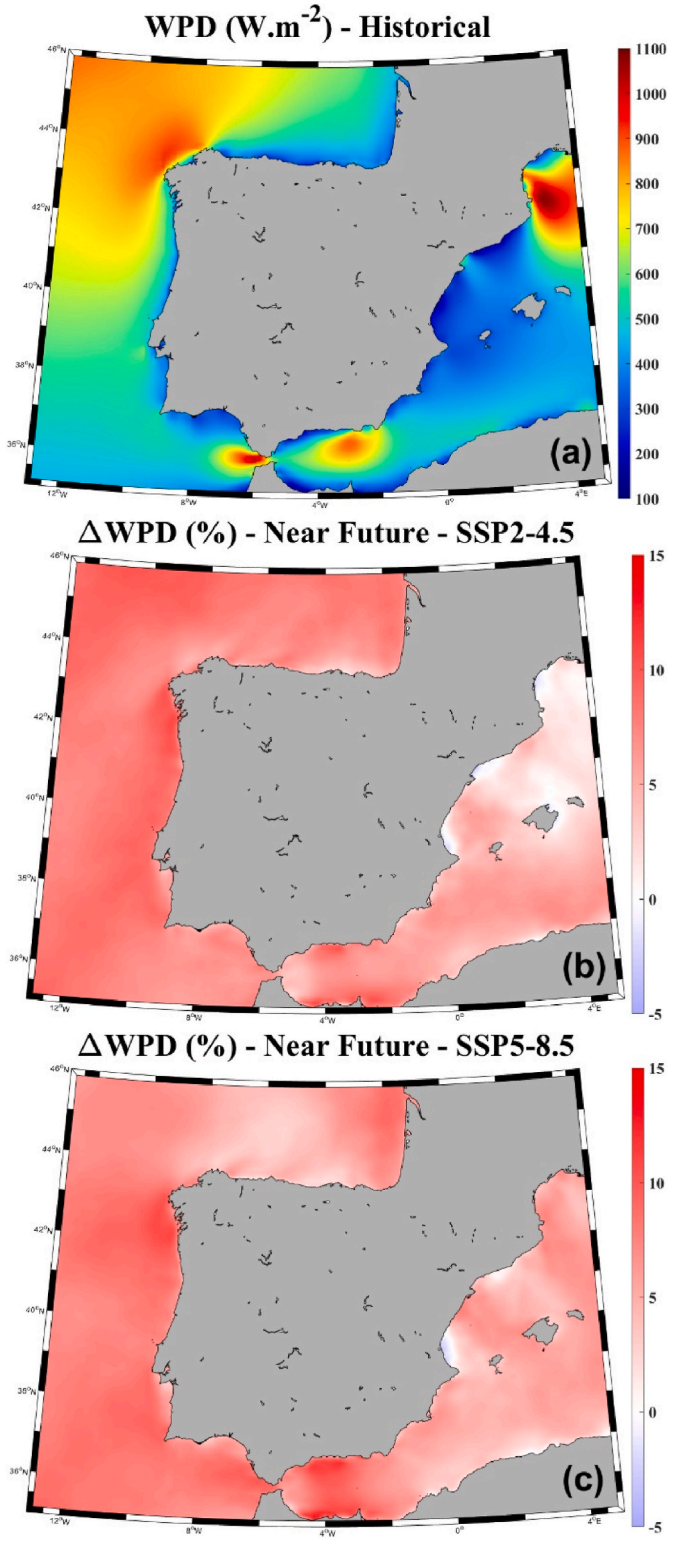

Fig. 6. **(a)** Mean WPD (W.m^{-2}) for the historical period (1985–2014), ΔWPD (%) for near future (2030–2059) under **(b)** the SSP2-4.5 and **(c)** SSP5-8.5 scenarios in the continental Spain and Balearic Islands.

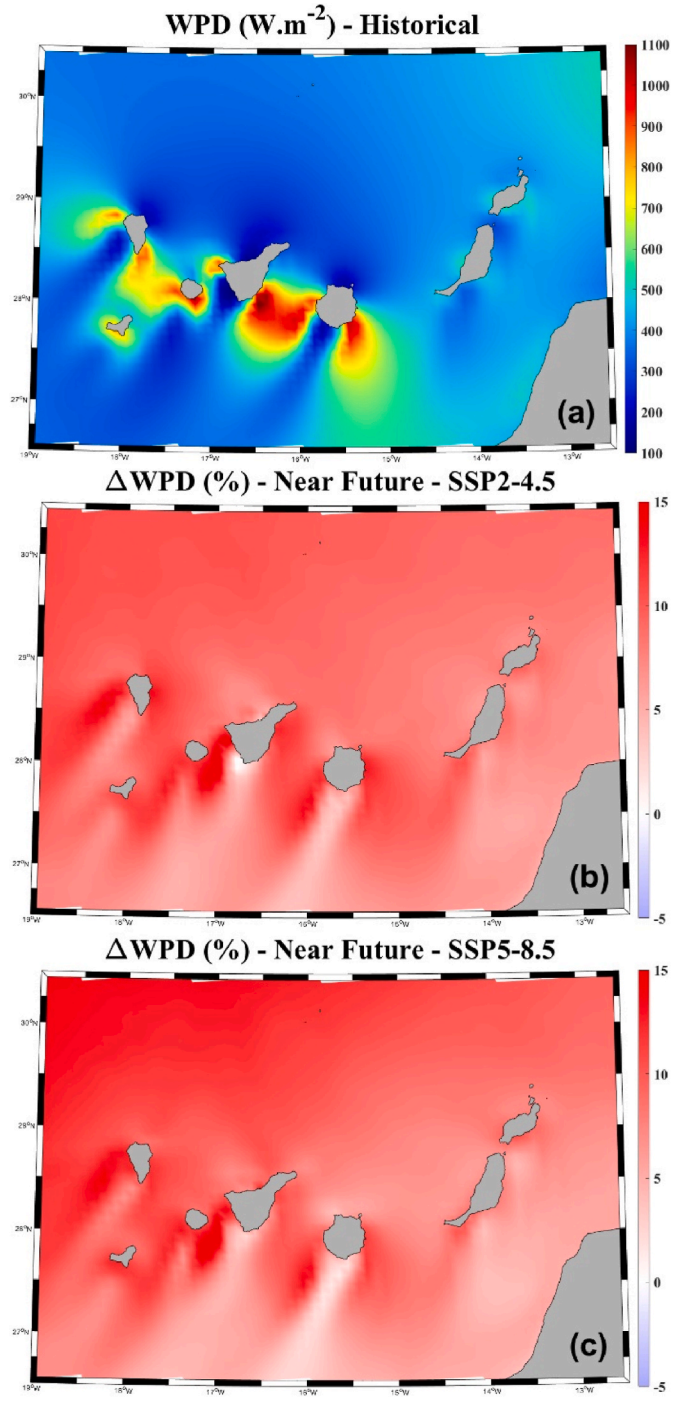

Fig. 7. **(a)** Mean WPD (W.m^{-2}) for the historical period (1985–2014), ΔWPD (%) for near future (2030–2059) under **(b)** the SSP2-4.5 and **(c)** SSP5-8.5 scenarios in the Canary Islands.

out in this study) makes it difficult for it to simulate these complex interactions. Thus, these low values of OP might not be caused by the WRF simulations, which might actually simulate the zone better than ERA5, thanks to a higher spatial resolution. González et al. (2017) also found low overlapping values in Tenerife island when they compared wind speed from WRF simulation with observed data in weather stations. Nevertheless, it is important to note that none of the Spanish MSP polygons are located within this zone. It is worth mentioning that OP values in this study are similar or slightly higher than those from previous analyses that validated wind speed from the CORDEX project. For instance, Costoya et al. (2020a) obtained similar OP values for the western Iberian Peninsula, while Costoya et al. (2021) obtained lower OP values in Chinese coastal waters. They compared their results with Cross-Calibrated Multi-Platform (CCMP) and ERA5 datasets, respectively.

The historical wind speed data obtained from WRF was also validated by comparing it with observational data from Puertos del Estado's

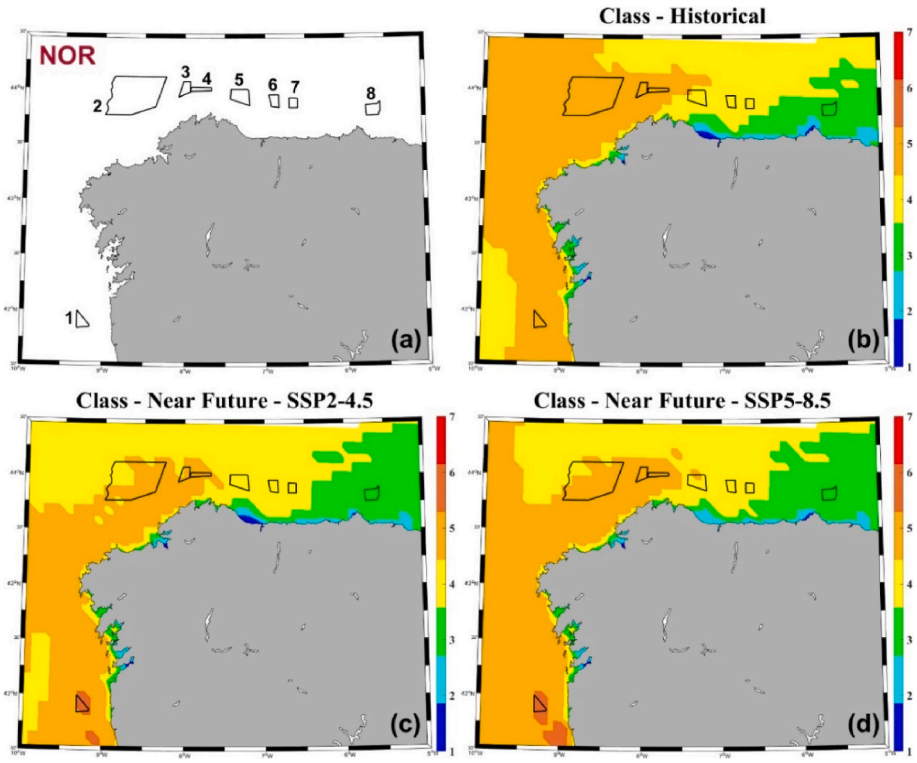

Fig. 8. **(a)** Locations and names of the polygons, **(b)** classification of the wind resource for the historical period (1985–2014), and for the near future (2030–2059) under **(c)** the SSP2-4.5 and **(d)** SSP5-8.5 scenarios in the NOR area.

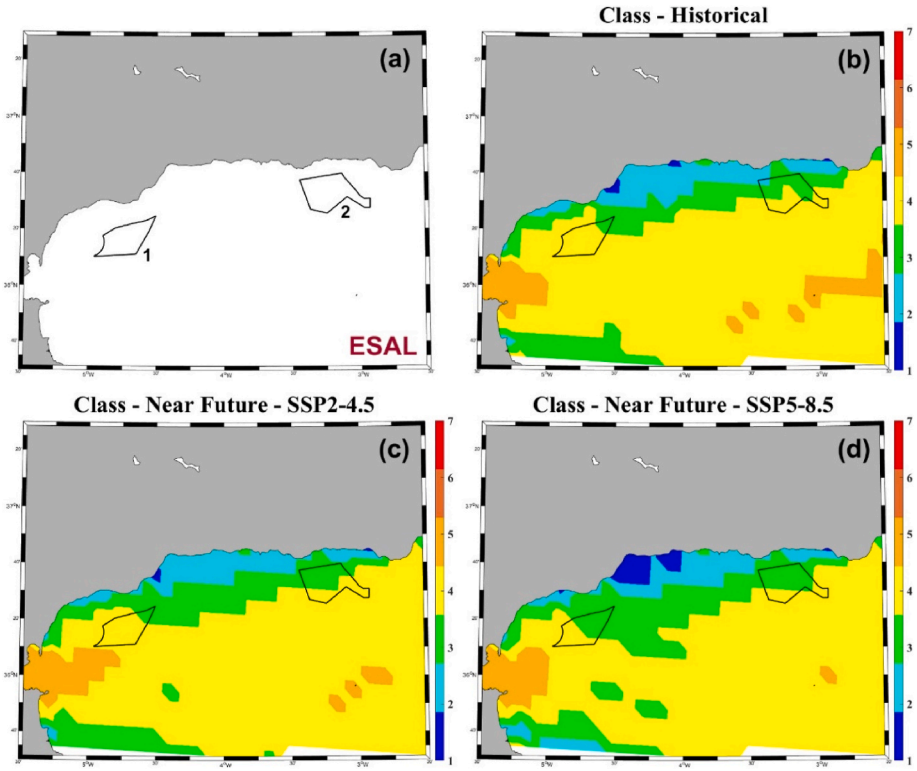

Fig. 9. **(a)** Locations and names of the polygons, **(b)** classification of the wind resource for the historical period (1985–2014), and for the near future (2030–2059) under **(c)** the SSP2-4.5 and **(d)** SSP5-8.5 scenarios in the ESAL area.

buoys. The comparison was done for W10, using the metrics described in section 2.2. The results are presented in Table 4. The OP values for half of the buoys were higher than 90%, while for the remaining buoys, it was higher than 85% (except for buoy 8, where OP was around 84%). The mean value of all buoys was close to 90%, and the standard deviation (3.7%) was relatively low. The ΔMed values oscillated

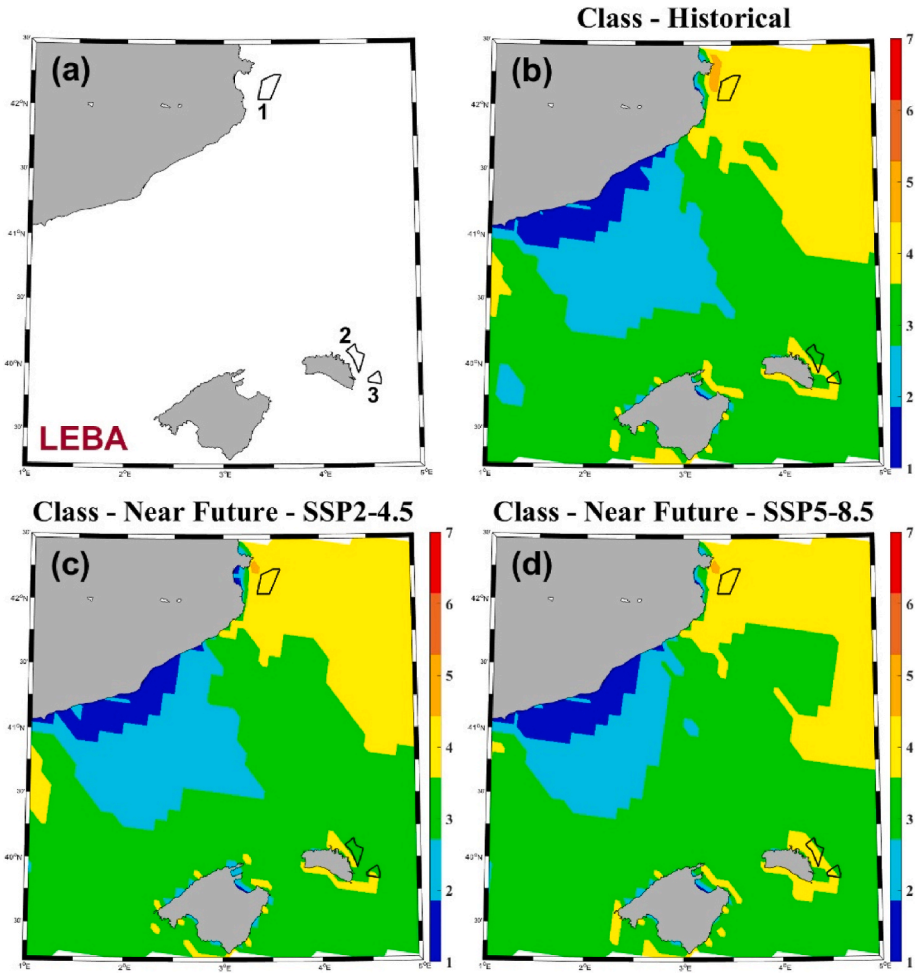

Fig. 10. **(a)** Locations and names of the polygons, **(b)** classification of the wind resource for the historical period (1985–2014), and for the near future (2030–2059) under **(c)** the SSP2-4.5 and **(d)** SSP5-8.5 scenario in the LEBA area.

approximately between 0 and 20% (in absolute value) and were all positive, except for buoy B14 (Gran Canaria). The average value for all buoys was around 10%, and the standard deviation was 8%, indicating a reasonably large interval. For ΔPeak, the absolute values were between 2% and 30%, and all were positive, except for the same B14 buoy. The mean value was approximately 15%, and the significant dispersion of the results was confirmed by a standard deviation of almost 12%. It is worth noting that, with the exception of buoy B14 located in Gran Canaria, all ΔMed and ΔPeak values are positive. This indicates that the WRF model tends to overestimate wind speeds in the Iberian Peninsula domain and underestimate them in the Canary Islands domain. Although some values of ΔMed and ΔPeak may appear high, they should be considered in context. For instance, if WRF estimates a median wind speed of 6 m s^{-1} while the buoy measures 5 m s^{-1}, the ΔMed value would be 20%. However, the actual difference between the two medians would only be 1 m s^{-1}. Moreover, the metrics at buoy number 14 location has also been calculated using data from ERA5 instead of WRF. The OP is lower than 65%, when ΔMed and ΔPeak values are around −25%. Thus, the results for the comparison between this buoy and WRF data are way better (Table 4), confirming that the low values of OP south of Tenerife island between WRF and ERA5 (Fig. 5b) are caused by a poorer accurate simulation from ERA5, not from WRF, in this area.

In their study, Costoya et al. (2020a) employed the same metrics as this investigation to compare their outcomes with buoys B2 to B6 in this research. The results indicate that this study's OP values are 5% higher than theirs, whereas their results showed a 2% improvement for ΔMed and a 0.5% improvement for ΔPeak. In Chinese territorial waters, Costoya et al. (2021) calculated the OP between their findings and W10 data from six buoys, and discovered a mean value of 87.9%, which is slightly lower than the value obtained in this work. Lastly, Costoya et al. (2020b) employed CORDEX data to model W10 in the coastal waters of the US. They obtained comparable results to those of this analysis, with an average OP value of 88.8% for 15 buoys in the US west coast, and 89.2% for 15 buoys in the US east coast.

Results of this study, which utilized WRF with CMIP6 data as boundary and initial conditions, demonstrate that the simulated wind speed values in the studied area are accurate. The study yielded OP values that were slightly higher than those of previous analyses that validated future projections from projects such as CORDEX with ERA5 and buoys data.

3.2. Impact of climate change on wind power density in a near future

Fig. 6a depicts the average WPD100 values during the 1985–2014 period in the Iberian Peninsula and Balearic Islands domain. The highest WPD is observed in the northwest of Spain (~900 W m^{-2}), the west part of the Strait of Gibraltar (~1000 W m^{-2}), west of Gate Cape (~900 W m^{-2}), and in the Gulf of Lion (~900–1100 W m^{-2}), whereas the lowest WPD is seen in the Mediterranean part of Spanish territorial waters, including Balearic Islands (~200–400 W m^{-2}). Similar findings were reported by Santos et al. (2018), who also identified the major WPD values in Galicia, the Strait of Gibraltar, and Cape Gata. Fig. 6b and c demonstrate the projected changes in WPD under SSP2-4.5 and SSP5-8.5 for the near future. The results indicate that a 15% increase in WPD is

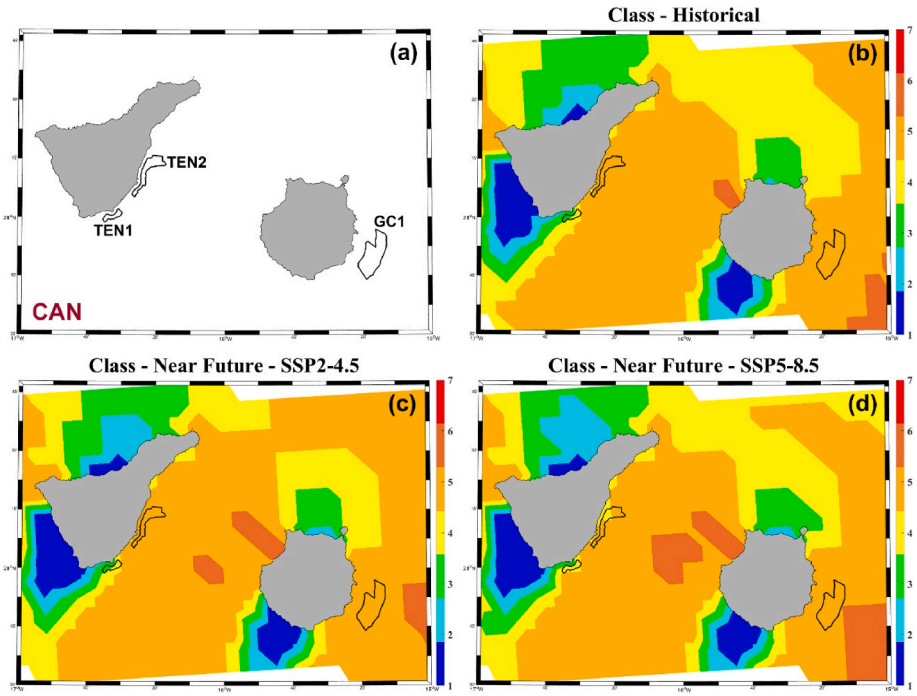

Fig. 11. **(a)** Locations and names of the polygons, **(b)** classification of the wind resource for the historical period (1985–2014), and for the near future (2030–2059) under **(c)** the SSP2-4.5 and **(d)** SSP5-8.5 scenarios in the western CAN area.

expected in all the waters of the Atlantic Ocean surrounding the Iberian Peninsula under SSP2-4.5, with a slightly higher increase in the Atlantic façade. Similar findings were reported by Fernández-Alvarez et al. (2023) for the 2049–2053 period. The WPD is expected to increase by approximately 15% at the eastern part of the Strait of Gibraltar. In the Mediterranean Sea, a 5–10% increase in WPD is anticipated, except for the waters between Mallorca and Menorca islands, where the resource is expected to remain constant as in the historical period. However, the WPD in coastal waters near Valencia and Barcelona may decrease by 5%. The projected results for the near future under SSP5-8.5 are very similar, except for a 5% increase in WPD at the Spanish north coast and the waters located between Mallorca and Menorca islands.

The mean WPD in the waters surrounding the Canary Islands during the historical period (1985–2014) is shown in Fig. 7a. The highest values were observed between the islands of La Palma and Gran Canaria (~750–1100 W m^{-2}), while the WPD was low at the northeast and southwest of the islands (~300–400 W m^{-2}). Around Fuerteventura and Lanzarote islands, the WPD was intermediate (~400–500 W m^{-2}). These findings are consistent with the simulation results reported by González et al. (2017) for the 1995–2004 period. The evolution of WPD during the near future under SSP2-4.5 (Fig. 7b) and SSP5-8.5 (Fig. 7c) scenarios shows a similar pattern. A 15% increase in WPD is expected between the islands and in the northern area, while the increase is expected to be only around 0–5% at the southeast of the islands. The lowest increase is predicted for Gran Canaria and Tenerife islands.

The findings of the study demonstrate that the WPD resource is susceptible to significant changes as a result of climate change, even in the near future. Consequently, it is insufficient to classify wind energy based solely on the historical period. It is necessary to consider both SSPs in the near future, as wind turbines will be generating energy during this period and will be affected by climate change. Furthermore, the study has computed the ΔWPD for the far future (2070–2099), which is presented in Fig. A1 and A2. Since the primary objective of the study is to assess the wind resource to facilitate the installation of offshore wind turbines in the near future, the figures for the far future are presented in the Appendix section. Under SSP2-4.5, Fig. A1a shows a similar pattern in the WPD changes in the Iberian Peninsula and the Balearic Islands for the far future than the one observed for the near future (Fig. 6b). Under SSP5-8.5, the changes in WPD are similar between near (Fig. 6c) and far (Fig. A1b) futures in the Atlantic Ocean, the Bay of Biscay and the Strait of Gibraltar. Nevertheless, a decrease in WPD up to −15% is expected during the far future in the Mediterranean Sea, especially at the Spanish East Coast and the Balearic Islands. In the Canary Islands, the pattern of changes in WPD is also highly similar between near (Fig. 7) and far (Fig. A2) futures. Nevertheless, in the areas where a small increase (around 0–5%) was expected for the near future, a decrease between −5% and −15% is obtained in the far future.

3.3. *Classification of the near future wind resource*

In this section, the offshore wind energy resource classification in the five areas included in the Spanish MSP (shown as red shapes in Fig. 1) is presented. Figs. 8–12 are provided, where subplot (a) shows the location and names of the polygons within the zone, subplot (b) displays the classification of the wind resource for the historical period, and subplots (c) and (d) show the classification for the near future period under the SSP2-4.5 and SSP5-8.5 scenarios, respectively. The classification has also been carried out for the far future under both SSPs and is shown in Figs. A3 to A7 in the Appendix section of this study.

Fig. 8 shows the wind energy resource classification for the NOR zone. Fig. 8b represents the historical period, where the classification appears to decrease from NOR1 to NOR8, with NOR1 to NOR4 classified as “excellent”, NOR5 to NOR7 as “good”, and NOR8 as “fair”. The classification for the near future is quite similar for both SSP2-4.5 (Fig. 8c) and SSP5-8.5 (Fig. 8d). The primary difference with the historical classification is that NOR1 is now classified as “outstanding”, and a portion of NOR2 is classified as “good” under both scenarios (~35% and ~20% under SSP2-4.5 and SSP5-8.5, respectively). An increase in WPD is expected for both NOR1 and NOR2 (Fig. 6b and c) in the future. Nevertheless, this increase combined to a high historical WPD in NOR2 (Fig. 6a) might result in too extreme wind speeds, thus a lower classification in the future, whereas in NOR1 the historical WPD is lower thus its increase in the future only results in a better classification. Costoya et al. (2022) also made the same classification for the 2000–2040 period,

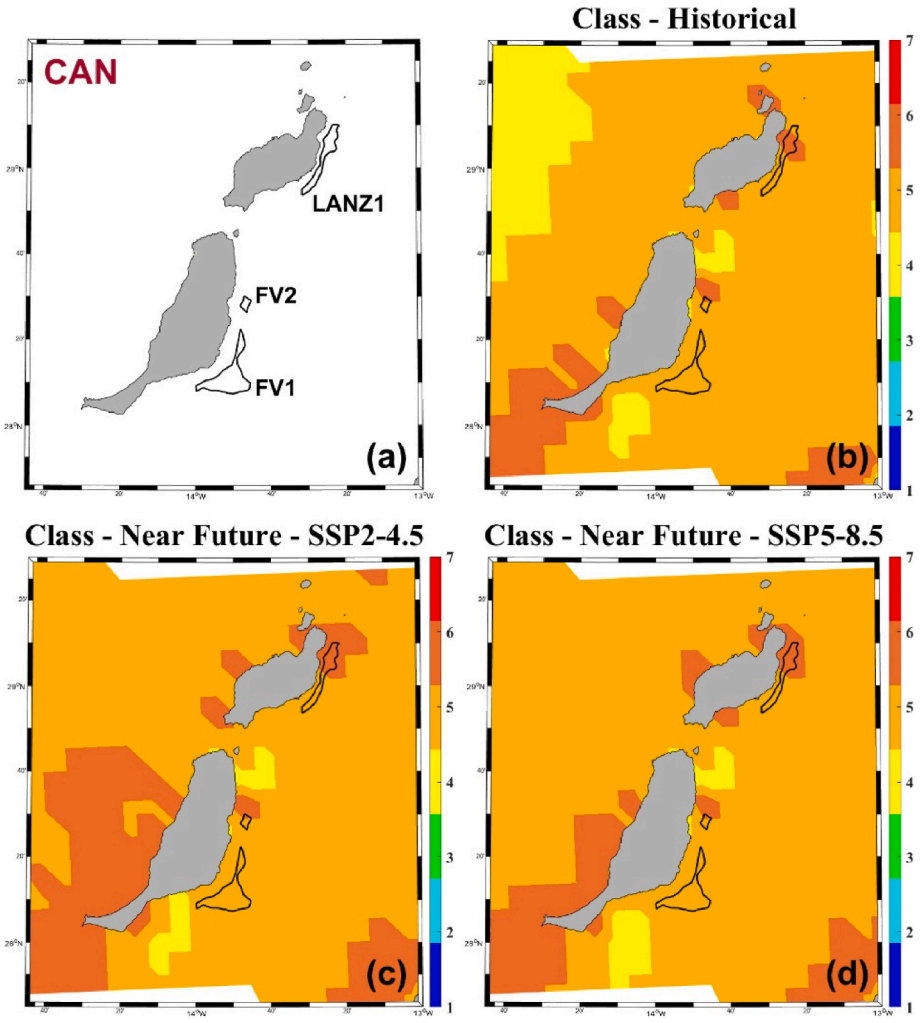

Fig. 12. **(a)** Locations and names of the polygons, **(b)** classification of the wind resource for the historical period (1985–2014), and for the near future (2030–2059) under **(c)** the SSP2-4.5 and **(d)** SSP5-8.5 scenarios in the eastern CAN area.

with similar results in this area. The results appear to be linked to the mean WPD and its evolution for the near future (see Fig. 6), as the resource is higher in the northwest corner of the Iberian Peninsula and decreases when following the Spanish north coast towards France.

The classification of offshore wind energy resource for the ESAL area is depicted in Fig. 9, which includes two polygons. For the historical period, shown in Fig. 9b, and the near future under SSP2-4.5, displayed in Fig. 9c, the majority of ESAL1 polygon is classified as "good" (~90%). However, in the near future under SSP5-8.5, as depicted in Fig. 9d, it is characterized as "fair/good" (in equal proportions), with the lower classification entering from the northeast direction. The ESAL2 polygon is also assessed as "fair/good" in all three simulations, with the lowest classification covering approximately 50%, 60% and 70% of the surface in historical, SSP2-4.5 and SSP5-8.5 simulations, respectively. It consistently spands its coverage in the southward direction. Even though Fig. 6 exhibits a substantial historical WPD for the entire ESAL area, with an expected 15% increase in the near future under both SSPs, the lower classification compared to the NOR area may be attributed to a less stable wind resource or extreme wind speeds.

The wind energy resource classification for the LEBA area is displayed in Fig. 10. The LEBA2 polygon is primarily classified as "fair", covering approximately 80% of the area during the historical period. Under SSP2-4.5, it is entirely classified as "fair," and under SSP5-8.5, it is classified as "good" over approximately 70% of its area. In contrast, the LEBA3 polygon is consistently classified as "fair/good" in both historical and SSP5-8.5 simulations, while only about 30% of its surface is classified as "good" under SSP2-4.5. The LEBA1 polygon is only classified as good in all three simulations, even though it is located in a zone with high WPD (Fig. 6). This suggests that, similar to the ESAL area, the resource's stability may be too low, and/or wind speeds too extreme.

In Fig. 11, the classification of the western part of the CAN area displays a wide range of values, ranging from poor to outstanding. This variability could be attributed to the high gradient of WPD observed in this region, as shown in Fig. 7a. The best classifications are located between the islands, whereas the worst are found at the north and southwest of the islands, which is consistent with the distribution of historical WPD values (Fig. 7a) and ΔWPD values (Fig. 7b and c). Regarding the CAN-TEN1 polygon, it is evenly classified as "fair/good" for the historical period (Fig. 11b) and the near future under SSP2-4.5 (Fig. 11c), while it is classified as "good" for the near future under SSP5-8.5 (Fig. 11d). On the other hand, both CAN-TEN2 and CAN-GC1 polygons are classified as "excellent" in all three simulations, with the exception of CAN-TEN2 under SSP5-8.5, where 30% of its surface is classified as "good".

Fig. 12 displays the classification of the eastern CAN area, which is well-classified overall. Despite the WPD resource in this region being only intermediate compared to other areas in the Canary Islands domain (Fig. 7a), the main part of the eastern CAN area is classified as "excellent", with some zones even considered "outstanding". Across all three simulations, the CAN-FV1 polygon is classified as "excellent", while both

Table 5
Classification of the wind resource for all polygons during the historical period (1985–2014) and the near future (2030–2059) under SSP2-4.5 and SSP5-8.5.

Polygon		Surface (km^2)	Historical	Near Future	
				SSP2-4.5	SSP5.8-5
NOR	1	117.63	Excellent	Superb	Superb
	2	1806.41	Excellent	Good	Good
	3	112.97	Excellent	Excellent	Excellent
	4	77.70	Excellent	Excellent	Excellent
	5	236.29	Good	Good	Good
	6	104.98	Good	Good	Good
	7	80.18	Good	Good	Good
	8	152.45	Fair	Fair	Fair
ESAL	1	534.24	Fair/Good	Fair/Good	Fair/Good
	2	688.37	Fair/Good	Fair/Good	Fair/Good
LEBA	1	249.99	Good	Good	Good
	2	147.35	Fair/Good	Fair	Fair/Good
	3	77.65	Fair/Good	Fair/Good	Fair/Good
CAN	TEN1	21.32	Fair/Good	Fair/Good	Good
	TEN2	70.78	Excellent	Excellent	Good/Excellent
	GC1	163.89	Excellent	Excellent	Excellent
	FV1	192.24	Excellent	Excellent	Excellent
	FV2	16.25	Excellent/Outstanding	Excellent/Outstanding	Excellent/Outstanding
	LANZ1	97.39	Excellent/Outstanding	Outstanding	Excellent/Outstanding

the CAN-FV2 and CAN-LANZ1 polygons are classified as "excellent/outstanding", in proportions 75%/25% and 50%/50%, respectively.

Table 5 summarizes the classification of all polygons for the historical period and near future simulations under both SSPs. The results indicate that NOR and CAN are generally the most suitable zones for wind turbine installation. The top-ranked polygons for wind turbine deployment are NOR1 and CAN-LANZ1, with outstanding classifications. The following best options would be NOR3, NOR4, CAN-GC1, CAN-FV1, and CAN-FV2. It can be noted that, despite an expected increase in WPD values in the near future (see Figs. 6 and 7), the wind resource classification in the polygons tends not to change between 1985-2014 and 2030–2059. These results are mainly due to an increase in extreme wind speeds (results not shown), that compensate the higher WPD resource in the classification values. Table A4 in the Appendix section displays the results for the far future simulations (2070–2099) under both SSPs. The results are quite similar than for the near future, except that a lower classification is expected in NOR1 and NOR2, and a better one in the CAN domain overall, especially under SSP5-8.5.

Figs. 8–12 represents the final classification value of the resource under different scenarios and periods. It is important to mention that climate change can impact this classification in various ways considering the different indices involved. Thus, modifications in wind speed patterns affect three of the four aspects used to classify wind energy (all except the economic one). Climate change directly modifies wind speed distributions, influencing the annual wind speed index. In the Spanish territorial waters (Figs. 6 and 7), it seems that the values of this index might increase due to climate change, along with the Rich Level Occurrence. Nevertheless, a significant increase in offshore wind energy magnitudes could potentially lead to a decline in indices such as the Extreme Wind Speed one. Finally, regarding the stability indices, a seasonal analysis should be performed to evaluate whether the increase in offshore wind speeds is uniform throughout the year.

4. Conclusions

The aim of this study was to assess the changes in the offshore wind energy potential in Spanish territorial waters over the course of the 21st century. Specifically, the focus was on classifying the wind energy potential in the areas designated for offshore wind farms as defined by the latest Spanish Maritime Spatial Planning. The wind energy classification developed in this study has a broader scope than merely considering wind power density when deciding where to install offshore wind turbines. Some areas may have high energetic potential, but they are not suitable for harnessing this resource, because of a high variability of the wind speeds, or values too extreme that could damage wind turbines. Therefore, the classification provides decision makers with information on the best polygons for wind turbine installation based not only on the quantity of energy that can be harnessed but also on other crucial aspects. These include the stability of the resource because electricity is needed throughout the year, the risk to wind turbines because they can be damaged under severe weather conditions and, the economic cost of installing because the cheaper the better. Combining all these factors into a single classification index is particularly valuable. Additionally, the study evaluates the impact of climate change on this classification, enabling decision makers to determine the suitability of polygons for wind energy harvesting in the future, not just based on historical data.

The study computed wind data in the targeted areas using the WRF dynamic downscaling of a multi-model ensemble from the CMIP6 project. The accuracy of these wind data was verified by comparing them with a reanalysis dataset and data gathered from buoys, and it was concluded that the simulated wind data in the studied area are reliable. Then, future projections under the SSP2-4.5 and SSP5-8.5 scenarios were considered. In summary, the key findings of this study are:

- There is a significant increase in the offshore wind energy potential expected throughout all of Spain's territorial waters in the near future, with particularly high increases in the Atlantic Ocean and most of the Canary archipelago waters. On the other hand, the Mediterranean Sea and southeastern areas of certain Canary Islands are expected to experience the lowest increases.
- The potential wind resource classification within the offshore wind farm areas displays a wide range from "fair" (3/7) to "outstanding" (6/7). The regions that hold the greatest promise for development in the near future are in the northwest of the Iberian Peninsula and the Canary Islands.

It should be noted that this whole analysis, here performed in the Spanish territorial waters, is applicable to every other area. Indeed, the CMIP6 multi-model ensemble used in this study offers data worldwide, which can identically be dynamically downscaled with the WRF atmospheric model. Moreover, many countries already defined a MSP for offshore wind energy, especially all of the European coastal countries.

Finally, it is crucial to keep in mind that wind turbines, which have their own operational and technical limitations, are needed for harnessing offshore wind energy. Thus, an interesting aspect, that has not been developed in this study, would be to consider the performance of various turbines under different simulated climatic conditions. In this regard, higher resolution simulation data may be necessary for polygons to obtain more accurate results.

CRediT authorship contribution statement

B. Thomas: Methodology, Software, Validation, Formal analysis, Data curation, Writing – original draft, Writing – review & editing, Visualization. **X. Costoya:** Conceptualization, Methodology, Software, Validation, Data curation, Writing – review & editing. **M. deCastro:** Conceptualization, Resources, Writing – review & editing, Supervision. **D. Insua-Costa:** Software, Writing – review & editing. **M. Senande-Rivera:** Software, Writing – review & editing. **M. Gómez-Gesteira:** Conceptualization, Resources, Supervision.

Declaration of competing interest

The authors declare that they have no known competing financial interests or personal relationships that could have appeared to influence the work reported in this paper.

Data availability

Data will be made available on request.

Acknowledgements

This work was partially supported by Xunta de Galicia under project ED431C 2021/44 (Grupos de Referencia Competitiva), Project TED2021-129479A-100 (SAFE project) funded by MCIN/AEI/10.13039/501100011033 and the "European Union NextGeneration EU/PRTR" and Project PID2021-128510OB-I00 (RIESPIRO) funded by MCIN/AEI. X. Costoya is funded by Grant IJC2020-043745-I (Juan de la Cierva Postdoctoral Fellowship) funded by MCIN/AEI/10.13039/501100011033 and by the "European Union NextGenerationEU/PRTR".

Computation took place at Finisterrae III supercomputer that belongs to CESGA (Centro de Supercomputación de Galicia) located at Santiago de Compostela, Galicia, Spain. Funding for open access charge: Universidade de Vigo/CISUG.

During the preparation of this work the authors used ChatGPT-3.5 in order to improve language and readability. After using this tool/service, the authors reviewed and edited the content as needed and take full responsibility for the content of the publication.

Appendix

- Normalization of the indices for classification

W_{ann} was normalized following the NREL classification (Table A1). DC and WD were normalized as specified in Table A2. The values for Tables A1 and A2 correspond to the ones found in various studies (Costoya et al., 2019, 2020b, 2021, 2022; Zheng and Pan, 2014; Zheng et al., 2018). The remaining indices were normalized following the procedure outlined in Costoya et al. (2022) as detailed in Table A3.

Table A1
Normalization of W_{ann}.

Normalized value	W_{ann} ($m.s^{-1}$)
0/6	<4.4
1/6	4.4–5.1
2/6	5.1–5.6
3/6	5.6–6
4/6	6–6.4
5/6	6.4–7
6/6	>7

Table A2
Normalization of distance to coast (DC) and water depth (WD) parameters.

Normalized value	DC (°)	WD (m)
0/4	>4	>500
1/4	3–4	100–500
2/4	2–3	50–100
3/4	0.5–2	25–50
4/4	<0.5	<25

Table A3
Normalization of EWSO, RLO, C_v, M_v and EWS parameters.

Normalized value	EWSO (%)	RLO (%)	C_v	M_v	EWS ($m.s^{-1}$)
0/9	<10	<10	>1.9	>2.5	>27
1/9	10–20	10–20	1.7–1.9	2.25–2.5	25.5–27
2/9	20–30	20–30	1.5–1.7	2–2.25	24–25.5
3/9	30–40	30–40	1.3–1.5	1.75–2	22.5–24
4/9	40–50	40–50	1.1–1.3	1.5–1.75	21–22.5
5/9	50–60	50–60	0.9–1.1	1.25–1.5	19.5–21
6/9	60–70	60–70	0.7–0.9	1–1.25	18–19.5
7/9	70–80	70–80	0.5–0.7	0.75–1	16.5–18
8/9	80–90	80–90	0.3–0.5	0.5–0.75	15–16.5
9/9	>90	>90	<0.3	<0.5	<15

- Impact of climate change on Wind Power Density in a far future

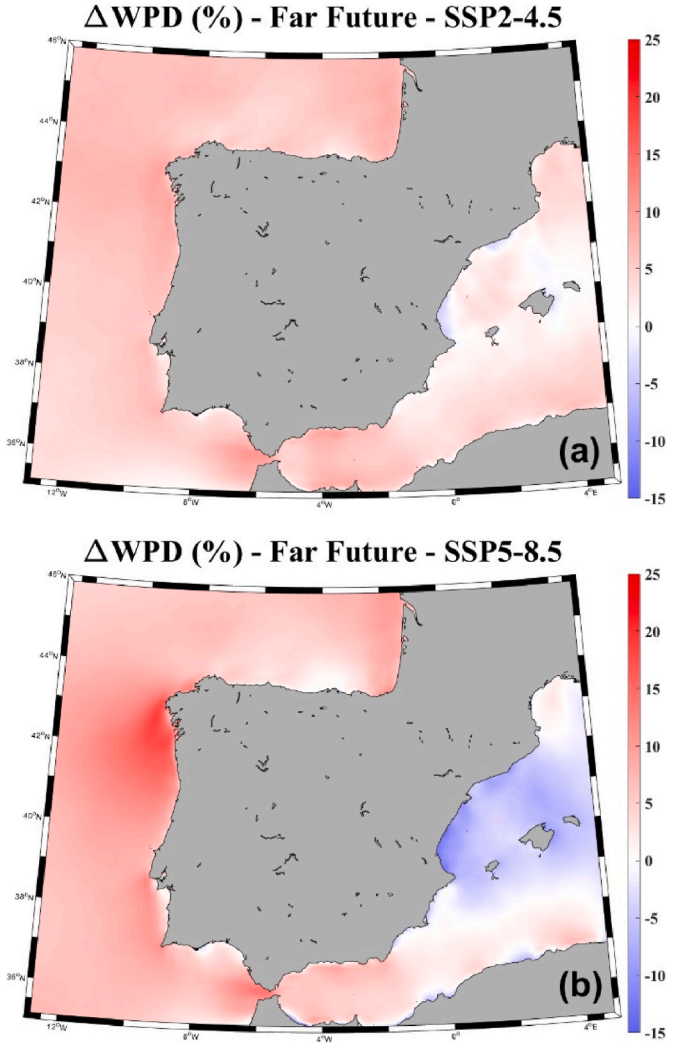

Fig. A1. Percentage of change in wind power density (ΔWPD) for the far future (2070–2099) **(a)** for the SSP2-4.5 scenario and **(b)** for the SSP5-8.5 scenario in the Continental Spain and Balearic Islands.

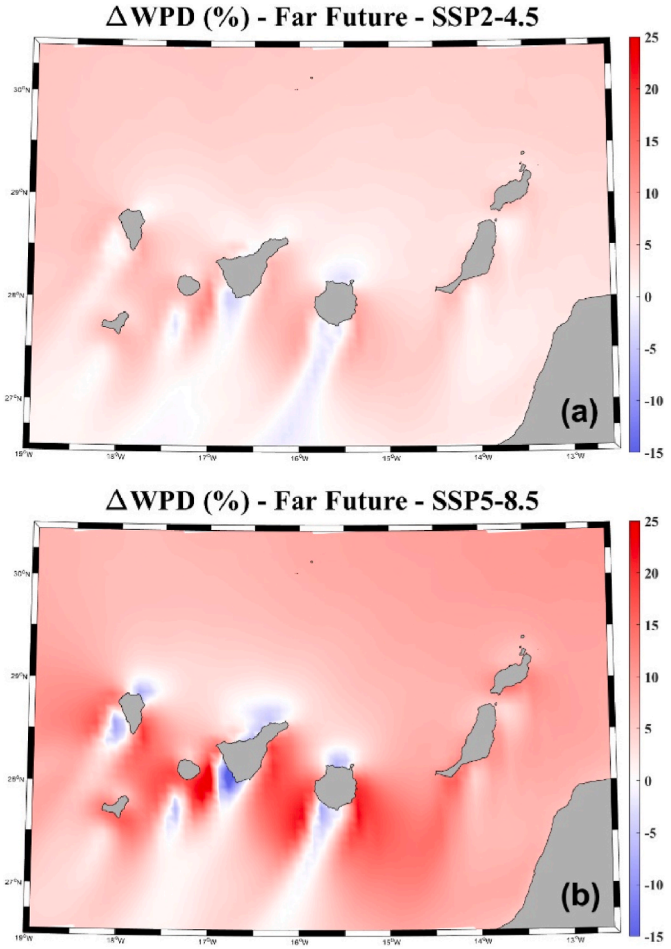

Fig. A2. Percentage of change in wind power density (ΔWPD) for the far future (2070–2099) **(a)** for the SSP2-4.5 scenario and **(b)** for the SSP5-8.5 scenario in the Canary Islands.

- Classification of the far future wind resource

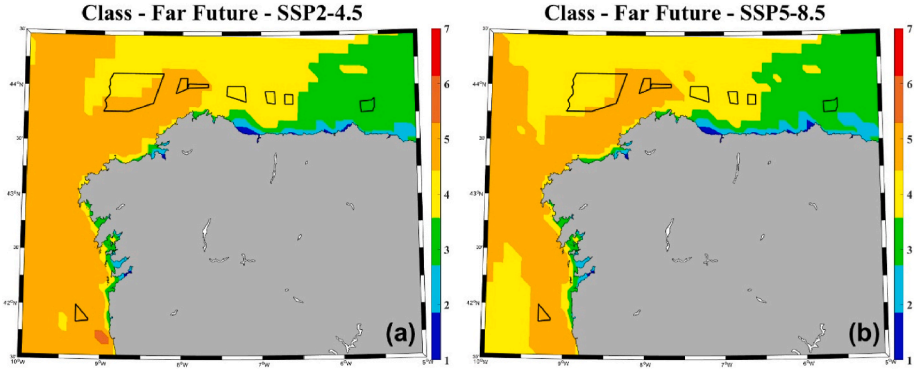

Fig. A3. Classification of the wind resource for the far future (2070–2099) under **(a)** SSP2-4.5 and **(b)** SSP5-8.5 scenarios in the NOR area.

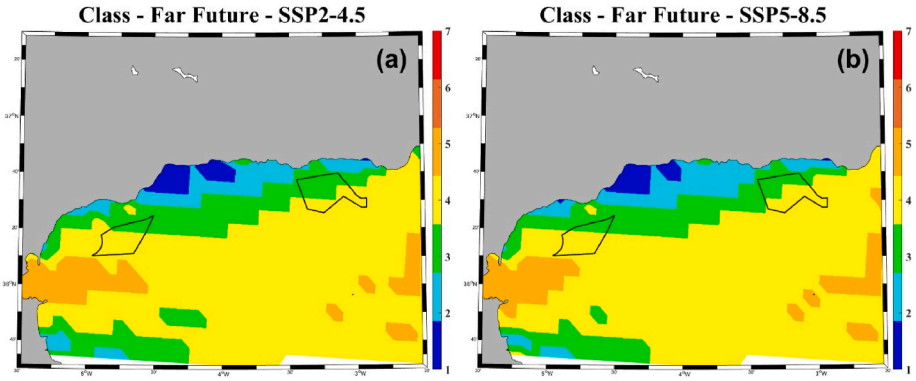

Fig. A4. Classification of the wind resource for the far future (2070–2099) under **(a)** SSP2-4.5 and **(b)** SSP5-8.5 scenarios in the ESAL area.

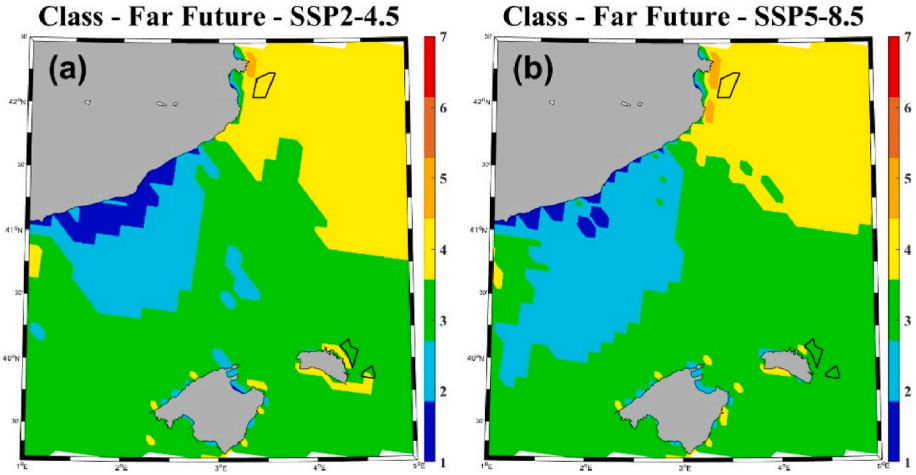

Fig. A5. Classification of the wind resource for the far future (2070–2099) under **(a)** SSP2-4.5 and **(b)** SSP5-8.5 scenarios in the LEBA area.

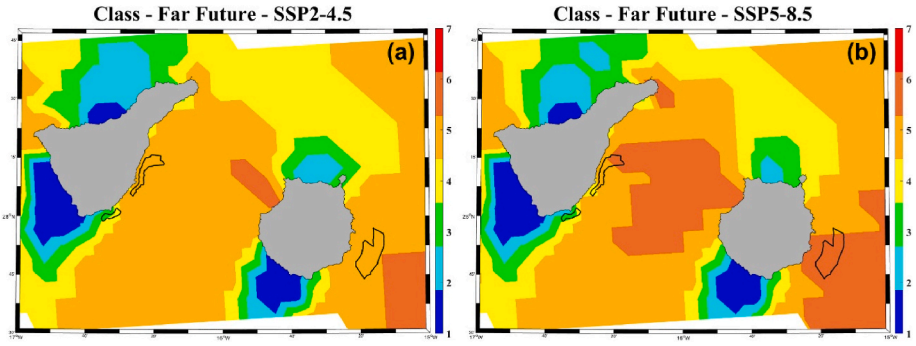

Fig. A6. Classification of the wind resource for the far future (2070–2099) under **(a)** SSP2-4.5 and **(b)** SSP5-8.5 scenarios in the western CAN area.

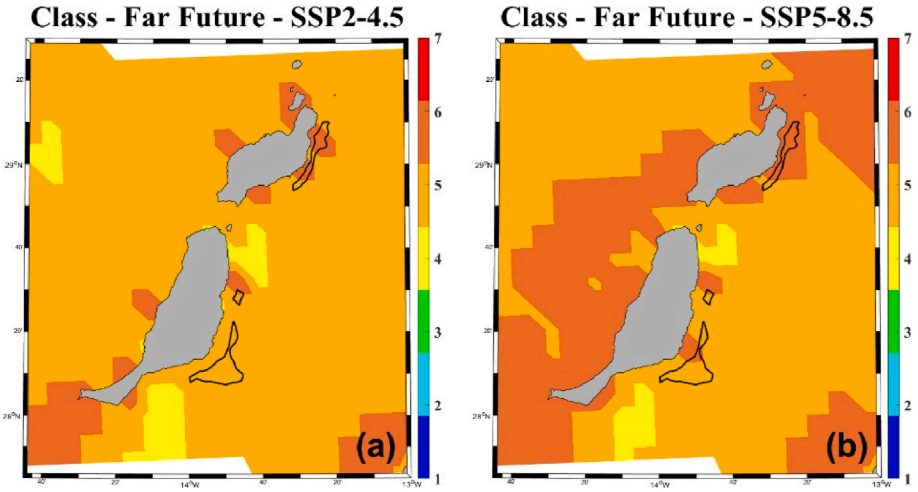

Fig. A7. Classification of the wind resource for the far future (2070–2099) under **(a)** SSP2-4.5 and **(b)** SSP5-8.5 scenarios in the eastern CAN area.

Table A4
Classification of the wind resource for all polygons during the far future (2070–2099) under SSP2-4.5 and SSP5-8.5.

Polygon		Far Future SSP2-4.5	Far Future SSP5.8-5
NOR	1	Excellent	Excellent
	2	Good	Good
	3	Excellent	Excellent
	4	Excellent	Excellent
	5	Good	Good
	6	Good	Good
	7	Good	Good
	8	Fair	Fair
ESAL	1	Fair	Fair
	2	Fair	Fair
LEBA	1	Good	Good
	2	Fair	Fair
	3	Fair	Fair
CAN	TEN1	Fair	Fair
	TEN2	Excellent	Good
	GC1	Excellent	Good
	FV1	Excellent	Excellent
	FV2	Excellent	Excellent
	LANZ1	Outstanding	Outstanding

Superb
Outstanding
Excellent
Good
Fair
Marginal
Poor

References

BOEM. Renewable energy on the outer continental shelf – offshore wind energy (n.d.). https://www.boem.gov/renewable-energy/renewable-energy-program-overview. (Accessed 7 July 2023).

Carvalho, D., Rocha, A., Costoya, X., DeCastro, M., Gómez-Gesteira, M., 2021. Wind energy resource over Europe under CMIP6 future climate projections: what changes from CMIP5 to CMIP6. Renew. Sustain. Energy Rev. 151, 111594 https://doi.org/10.1016/j.rser.2021.111594.

Castro-Santos, L., Diaz-Casas, V., 2015. Economic influence of location in floating offshore wind farms. Ocean Eng. 107, 13–22. https://doi.org/10.1016/j.oceaneng.2015.07.025.

Castro-Santos, L., Filgueira-Vizoso, A., Carral-Couce, L., Formoso, J.Á.F., 2016. Economic feasibility of floating offshore wind farms. Energy 112, 868–882. https://doi.org/10.1016/j.energy.2016.06.135.

Costoya, X., deCastro, M., Santos, F., Sousa, M.C., Gómez-Gesteira, M., 2019. Projections of wind energy resources in the Caribbean for the 21st century. Energy 178, 356–367. https://doi.org/10.1016/j.energy.2019.04.121.

Costoya, X., Rocha, A., Carvalho, D., 2020a. Using bias-correction to improve future projections of offshore wind energy resource: a case study on the Iberian Peninsula. Appl. Energy 262, 114562. https://doi.org/10.1016/j.apenergy.2020.114562.

Costoya, X., deCastro, M., Carvalho, D., Gómez-Gesteira, M., 2020b. On the suitability of offshore wind energy resource in the United States of America for the 21st century. Appl. Energy 262, 114537. https://doi.org/10.1016/j.apenergy.2020.114537.

Costoya, X., deCastro, M., Carvalho, M., Feng, Z., Gómez-Gesteira, M., 2021. Climate change impacts on the future offshore wind energy resource in China. Renew. Energy 175, 731–747. https://doi.org/10.1016/j.renene.2021.05.001.

Costoya, X., deCastro, M., Carvalho, D., Arguilé-Pérez, B., Gómez-Gesteira, M., 2022. Combining offshore wind and solar photovoltaic energy to stabilize energy supply under climate change scenarios: a case study on the western Iberian Peninsula. Renew. Sustain. Energy Rev. 157, 112037 https://doi.org/10.1016/j.rser.2021.112037.

Díaz, H., Fonseca, R.B., Guedes Soares, C., 2019. Site selection process for floating offshore wind farms in Madeira Islands. In: Advances in Renew. Energies Offshore, pp. 729–737. In: https://www.researchgate.net/profile/Hugo-Diaz-3/publication/328289917_Site_selection_process_for_floating_offshore_wind_farms_in_Madeira_Islands/links/5bc4a9aaa6fdcc2c91fc508c/Site-selection-process-for-floating-offshore-wind-farms-in-Madeira-Islands.pdf. (Accessed 9 October 2023).

Eyring, V., Bony, S., Meehl, G.A., Senior, C.A., Stevens, B., Stouffer, R.J., et al., 2016. Overview of the coupled model Intercomparison project phase 6 (CMIP6) experimental design and organization. Geosci. Model Dev. (GMD) 9 (5), 1937–1958. https://doi.org/10.5194/gmd-9-1937-2016.

Fernández-Alvarez, J.C., Costoya, X., Pérez-Alarcón, A., Rahimi, S., Nieto, R., Gimeno, L., 2023. Dynamic downscaling of wind speed over the North Atlantic Ocean using CMIP6 projections: implications for offshore wind power density. Energy Rep. 9, 873–885. https://doi.org/10.1016/j.egyr.2022.12.036.

González, A., Pérez, J.C., Díaz, J.P., Expósito, F.J., 2017. Future projections of wind resource in a mountainous archipelago, Canary Islands. Renew. Energy 104, 120–128. https://doi.org/10.1016/j.renene.2016.12.021.

GWEC, 2020. Global Offshore Wind Report 2020. https://gwec.net/global-offshore-wind-report-2020/. (Accessed 7 July 2023).

GWEC, 2023. Global Offshore Wind Report 2022. https://gwec.net/gwecs-global-offshore-wind-report/. (Accessed 7 July 2023).

Hersbach, H., Bell, B., Berrisford, P., Hirahara, S., Horányi, A., Muñoz-Sabater, J., et al., 2020. The ERA5 global reanalysis. Q. J. R. Meteorol. Soc. 146 (730), 1999–2049. https://doi.org/10.1002/qj.3803.

Hong, S.-Y., Noh, Y., Dudhia, J., 2006. A new vertical diffusion package with an explicit treatment of entrainment processes. Mon. Weather Rev. 134 (9), 2318–2341. https://doi.org/10.1175/MWR3199.1.

Horvath, K., Koracin, D., Vellore, R., Jiang, J., Belu, R., 2012. Sub-kilometer dynamical downscaling of near-surface winds in complex terrain using WRF and MM5 mesoscale models. J. Geophys. Res. Atmos. 117 (11), D11111 https://doi.org/10.1029/2012JD017432.

Iacono, M.J., Delamere, J.S., Mlawer, E.J., Shepard, M.W., Clough, S.A., Collins, W.D., 2008. Radiative forcing by long-lived greenhouse gases: calculations with the AER radiative transfer models. J. Geophys. Res. Atmos. 113 (13), D13103 https://doi.org/10.1029/2008JD009944.

IEA, 2023. Renewable Energy Market Update – Outlook for 2023 and 2024. https://iea.blob.core.windows.net/assets/63c14514-6833-4cd8-ac53-f9918c2e4cd9/RenewableEnergyMarketUpdate_June2023.pdf. (Accessed 10 October 2023).

IPCC, 2021. Climate Change 2021 - the Physical Science Basis - Summary for Policymakers. https://www.ipcc.ch/report/ar6/wg1/downloads/report/IPCC_AR6_WGI_SPM_final.pdf. (Accessed 7 July 2023).

Jerez, S., López-Romero, J.M., Turco, M., Lorente-Plazas, R., Gómez-Navarro, J.J., Jiménez-Guerrero, P., et al., 2020. On the spin-up period in WRF simulations over Europe: trade-offs between length and seasonality. J. Adv. Model. Earth Syst. 12, 4. https://doi.org/10.1029/2019MS001945.

Jiménez, P.A., Dudhia, J., González-Rouco, J.F., Navarro, J., Montávez, J.P., García-Bustamante, E., 2012. A revised scheme for the WRF surface layer formulation. Mon. Weather Rev. 140 (3), 898–918. https://doi.org/10.1175/MWR-D-11-00056.1.

Lo, J.C.-F., Yang, Z.-L., Pielke, Sr, RA, 2008. Assessment of three dynamical climate downscaling methods using the Weather Research and Forecasting (WRF) model. J. Geophys. Res. Atmos. 113 (9), D09112 https://doi.org/10.1029/2007JDO09216.

Martinez, A., Murphy, L., Iglesias, G., 2023. Evolution of offshore wind resources in Northern Europe under climate change. Energy 269, 126655. https://doi.org/10.1016/j.energy.2023.126655.

Pan, Z., Takle, E., Gutowski, W., Turner, R., 1999. Long simulation of regional climate as a sequence of short segments. Mon. Weather Rev. 127 (3), 308–321. https://doi.org/10.1175/1520-0493(1999)127%3C0308:LSORCA%3E2.0.CO;2.

Peixoto, J.P., Oort, A.H., 1992. Physics of Climate. American Institute of Physics, New York.

Perkins, S.E., Pitman, A.J., Holbrook, N.J., McAneney, J., 2007. Evaluation of the AR4 climate Models' simulated daily maximum temperature, minimum temperature, and precipitation over Australia using probability density functions. J. Clim. 20 (17), 4356–4376. https://doi.org/10.1175/JCLI4253.1.

Qian, J.H., Seth, A., Zebiak, S., 2003. Reinitialized versus continuous simulations for regional climate downscaling. Mon. Weather Rev. 131 (11), 2857–2874. https://doi.org/10.1175/1520-0493(2003)131%3C2857:RVCSFR%3E2.0.CO;2.

Riahi, K., Van Vuuren, D.P., Kriegler, E., Edmonds, J., O'Neill, B.C., Fujimori, S., et al., 2017. The Shared Socioeconomic Pathways and their energy, land use, and greenhouse gas emissions implications: an Overview. Glob. Environ. Change 42, 153–168. https://doi.org/10.1016/j.gloenvcha.2016.05.009.

Ribeiro, A.S., deCastro, M., Costoya, X., Rusu, L., Dias, J.M., Gomez-Gesteira, M., 2021. A Delphi method to classify wave energy resource for the 21st century: application to the NW Iberian Peninsula. Energy 235, 121396. https://doi.org/10.1016/j.energy.2021.121396.

Rodríguez-Rodríguez, D., Malak, D.A., Soukissian, T., Sánchez-Espinosa, A., 2016. Achieving Blue Growth through maritime spatial planning: offshore wind energy optimization and biodiversity conservation in Spain. Mar. Pol. 73, 8–14. https://doi.org/10.1016/j.marpol.2016.07.022.

Salvação, N., Guedes Soares, C., 2018. Wind resource assessment offshore the Atlantic Iberian coast with the WRF model. Energy 145, 276–287. https://doi.org/10.1016/j.energy.2017.12.101.

Salvador, S., Costoya, X., Sanz-Larruga, F.J., Gimeno, L., 2018. Development of offshore wind power: contrasting optimal wind sites with legal restrictions in Galicia, Spain. Energies 11 (4), 731. https://doi.org/10.3390/en11040731.

Santos, F., Gómez-Gesteira, M., Añel, J.A., de Castro, M., Carvalho, D., Costoya, X., et al., 2018. On the accuracy of CORDEX RCMs to project future winds over the Iberian Peninsula and surrounding ocean. Appl. Energy 228, 289–300. https://doi.org/10.1016/j.apenergy.2018.06.086.

Skamarock, W.C., Klemp, J.B., Dudhia, J., Gill, D.O., Liu, Z., Berner, J., et al., 2021. A Description of the Advanced Research WRF Model Version 4. NCAR/TN-556+STR. https://doi.org/10.5065/1dfh-6p97.

Soares, P.M.M., Lima, D.C.A., Cardoso, R.M., Nascimento, M.L., Semedo, A., 2017. Western Iberian offshore wind resources: more or less in a global warming climate? Appl. Energy 203, 72–90. https://doi.org/10.1016/j.apenergy.2017.06.004.

Spanish Ministry for Ecological Transition and the Demographical Challenge, 2022. Roadmap Offshore Wind and Marine Energy in Spain. https://www.miteco.gob.es/es/ministerio/planes-estrategias/desarrollo-eolica-marina-energias/enhreolicamarina-pdf_accesible_tcm30-538999.pdf. (Accessed 7 July 2023).

Spanish Ministry for Ecological Transition and the Demographical Challenge, 2023. Marine Spatial Planning. https://www.miteco.gob.es/es/prensa/230201poemcmin_tcm30-559832.pdf. (Accessed 7 July 2023).

Tewari, M., Chen, F., Wang, W., Dudhia, J., LeMone, M.A., Mitchell, K., et al., 2004. Implementation and verification of the unified noah land surface model in the WRF model. Bull. Am. Meteorol. Soc. 2165–2170.

Thompson, G., Field, P.R., Rasmussen, R.M., Hall, W.D., 2008. Explicit forecasts of winter precipitation using an improved bulk microphysics scheme. Part II: implementation of a new snow parametrization. Mon. Weather Rev. 136 (12), 5095–5115. https://doi.org/10.1175/2008MWR2387.1.

United Nations, 2021. COP26 - Together for Our Planet. https://www.un.org/en/climatechange/cop26. (Accessed 7 July 2023).

WindEurope, 2022. Offshore Wind in EU Maritime Spatial Plans. https://windeurope.org/intelligence-platform/product/offshore-wind-in-eu-maritime-spatial-plans/. (Accessed 7 July 2023).

WindEurope, 2023a. Wind Energy in Europe: 2022 Statistics and the Outlook for 2023-2027. https://windeurope.org/intelligence-platform/product/wind-energy-in-europe-2022-statistics-and-the-outlook-for-2023-2027/. (Accessed 7 July 2023).

WindEurope, 2023b. Offshore Wind Energy. https://windeurope.org/policy/topics/offshore-wind-energy/. (Accessed 7 July 2023).

Xu, Z., Han, Y., Tam, C.-Y., Yang, Z.-L., Fu, C., 2021. Bias-corrected CMIP6 global dataset for dynamical downscaling of the historical and future climate (1979–2100). Sci. Data 8, 293. https://doi.org/10.1038/s41597-021-01079-3.

Zhang, C., Wang, Y., 2017. Projected future changes of tropical cyclone activity over the Western North and South pacific in a 20-km-Mesh regional climate model. J. Clim. 30 (15), 5923–5941. https://doi.org/10.1175/JCLI-D-16-0597.1.

Zhang, S., Li, X., 2021. Future projections of offshore wind energy resources in China using CMIP6 simulations and a deep learning-based downscaling method. Energy 217, 119321. https://doi.org/10.1016/j.energy.2020.119321.

Zheng, C.W., Pan, J., 2014. Assessment of the global ocean wind energy resource. Renew. Sustain. Energy Rev. 33, 382–391. https://doi.org/10.1016/j.rser.2014.01.065.

Zheng, C.W., Xiao, Z.N., Peng, Y.H., Li, C.Y., Du, Z.B., 2018. Rezoning global offshore wind energy resources. Renew. Energy 129, 1–11. https://doi.org/10.1016/j.renene.2018.05.090.